Supplementary data

Integration of catalytic capability and pH-responsive wettability conducted by V_xO_y-based dual-mesh system: towards solving trade-off between separation flow rate and degradation efficiency

*Ya'nan Liu, Ruixiang Qu, Xiangyu Li, Huajun Zhai, Shuaiheng Zhao, Yen Wei and Lin Feng**

Department of Chemistry, Tsinghua University, Beijing, 100084, P. R. China.

E-mail: fl@mail.tsinghua.edu.cn

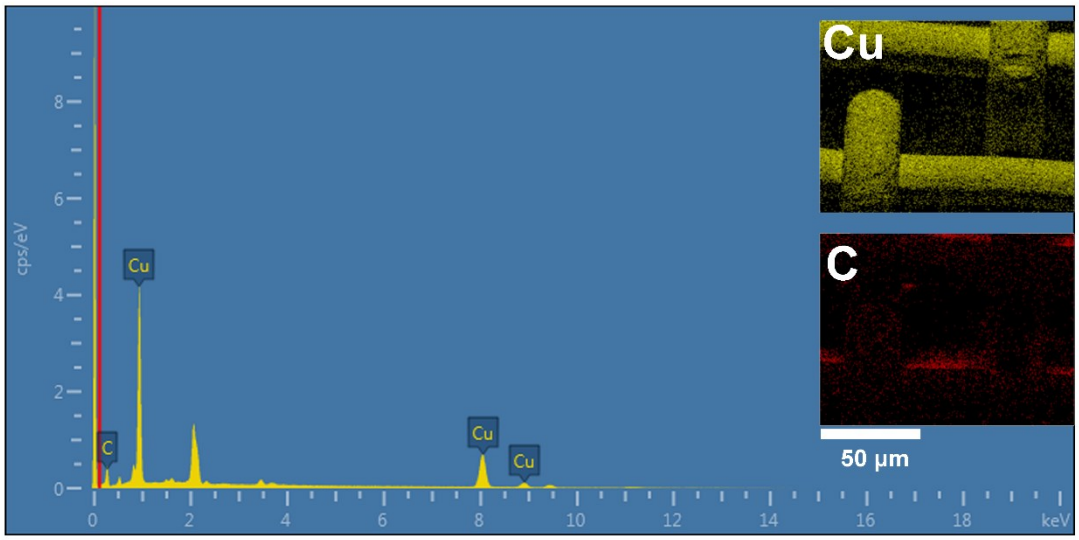

Fig. S1. EDX results of Cu substrate.

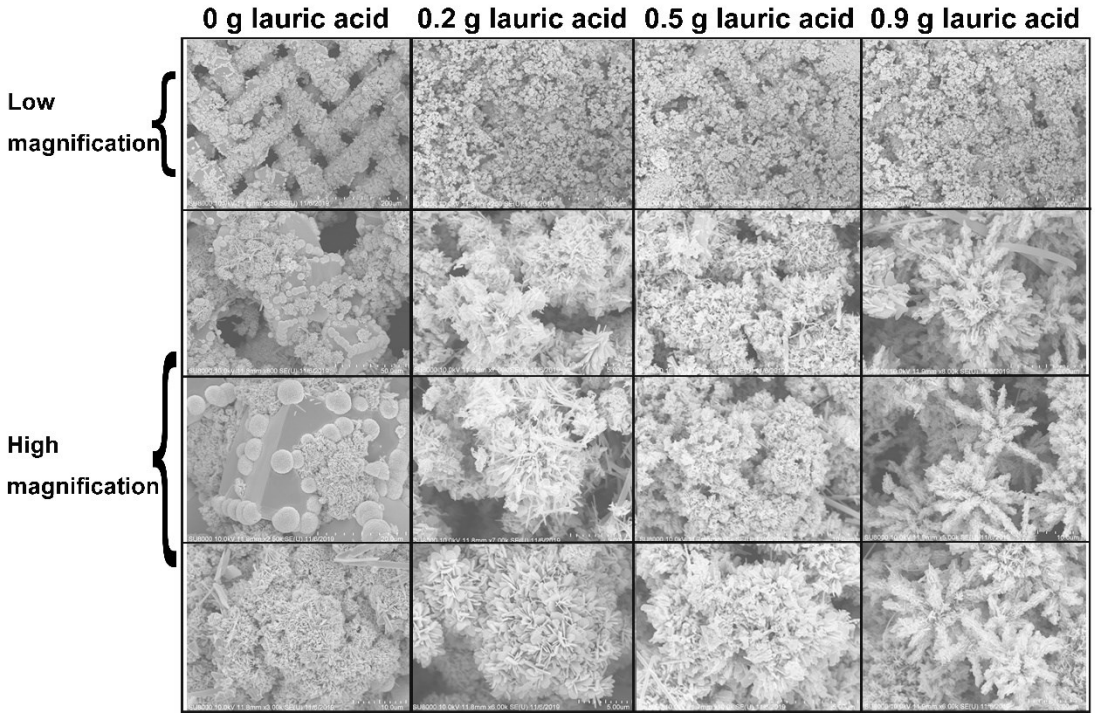

Fig. S2. The morphology differences among 0 g, 0.2 g, 0.5 g, 0.9 g lauric acid-doped V_xO_y groups. With the doping amount of lauric acid increased, the dispersion of V_xO_y spheres inclines to be uniform and the branches of subunits show more clear orientations and patterns.

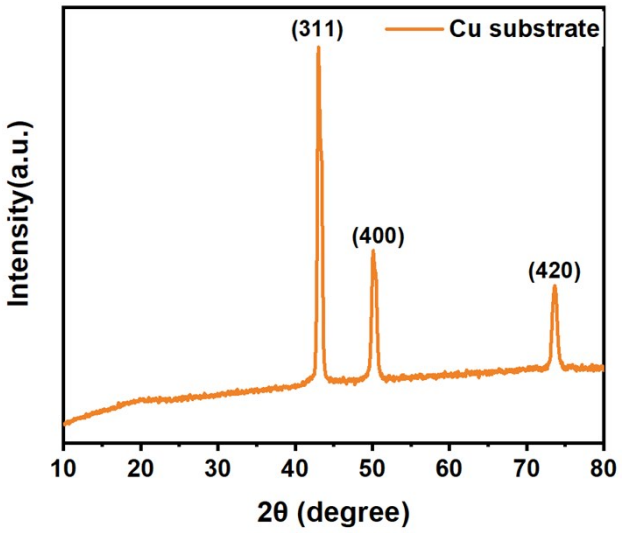

Fig. S3. XRD pattern of Cu substrate.

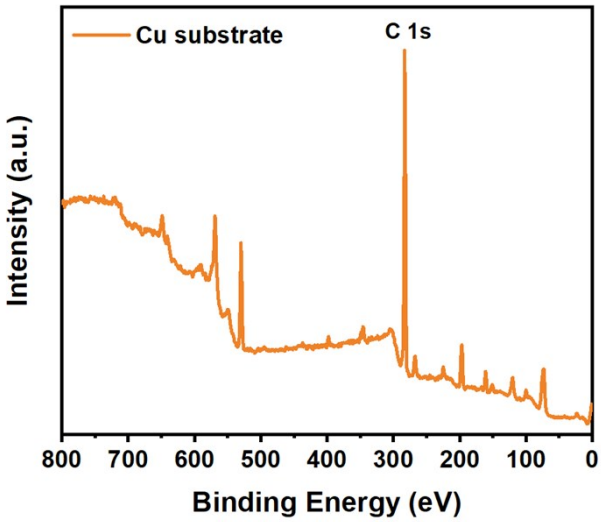

Fig. S4. Wide-scan XPS spectra of Cu substrate.

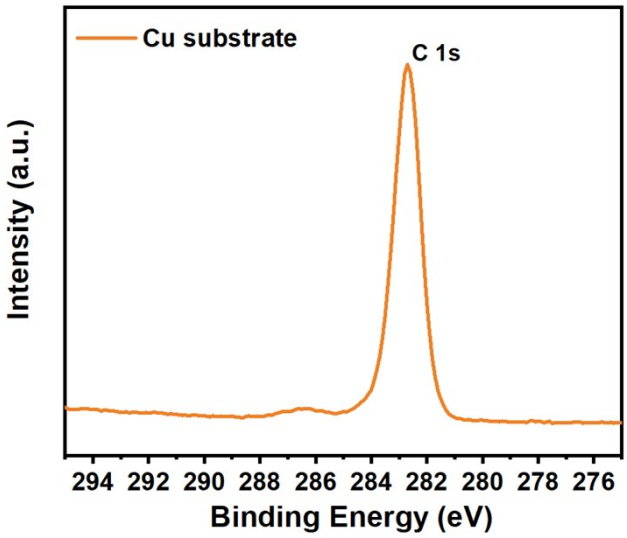

Fig. S5. Narrow-scan XPS spectra of C 1s peak of Cu substrate.

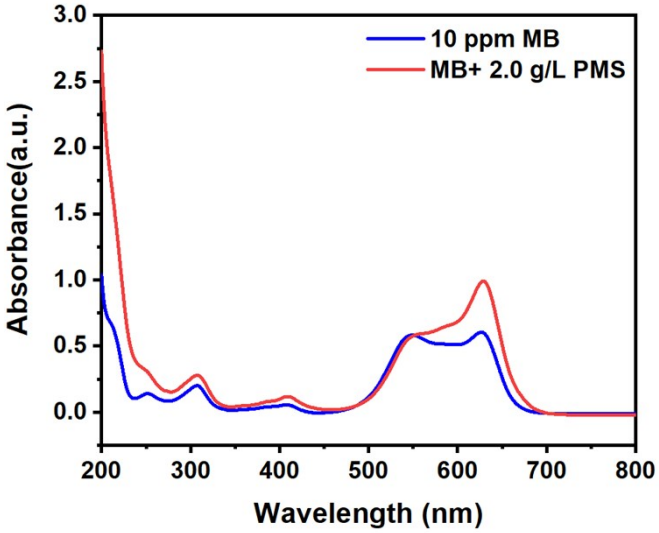

Fig. S6. UV-Vis spectra of 10 ppm MB that was solely treated by 2.0 g/L PMS.

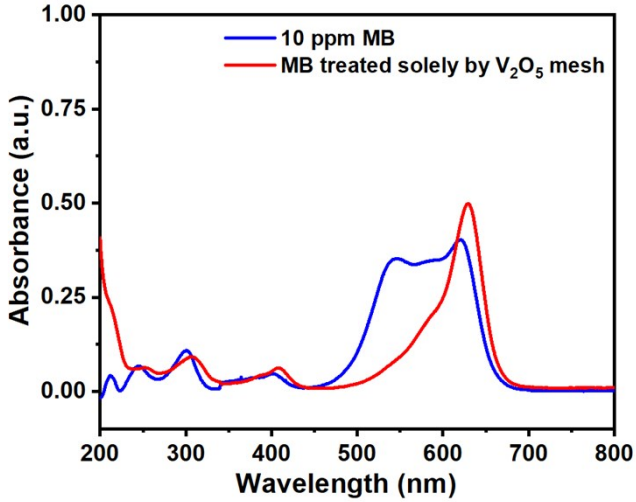

Fig. S7. UV-Vis spectra of 10 ppm MB that was solely treated by V_2O_5 mesh.

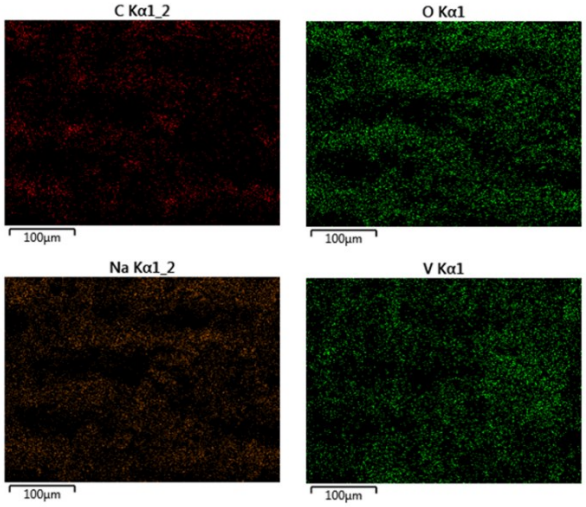

Fig. S8. EDX spectra of the switch mesh that was treated by pH =12 NaOH.

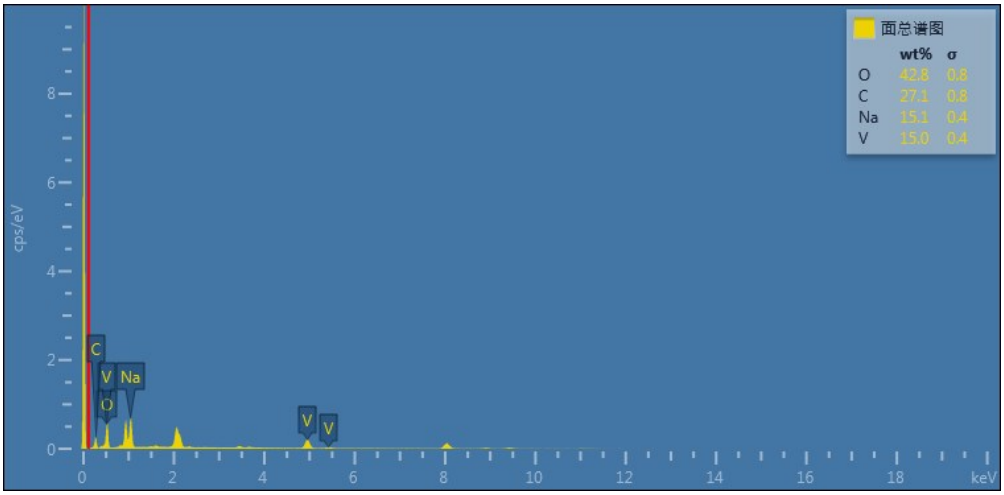

Fig. S9. Mapping results from Fig. S6.

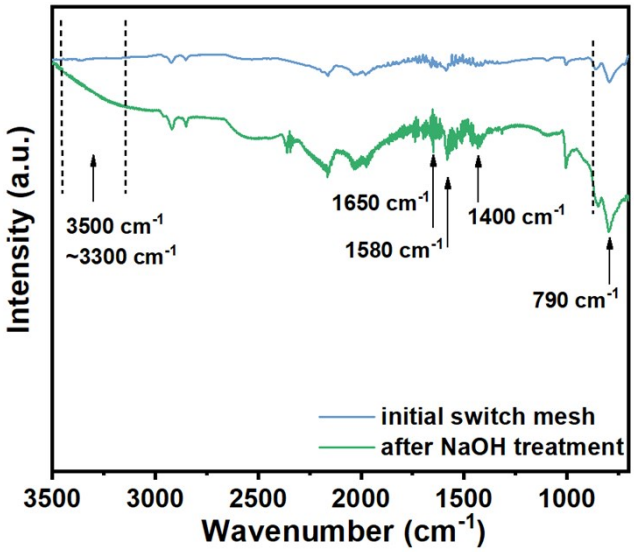

Fig. S10. FTIR spectra of the switch mesh before and after treatment by pH= 12 NaOH.

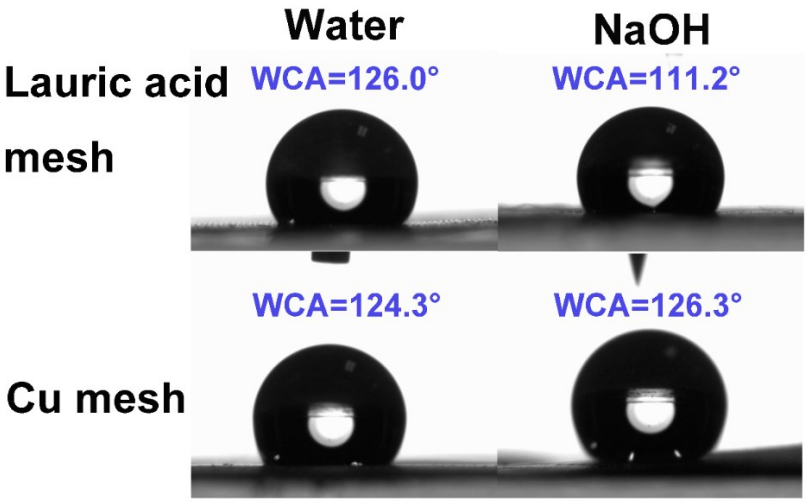

Fig. S11. Water contact angles of lauric acid-mesh and Cu substrate in air in neutral and alkaline environments.

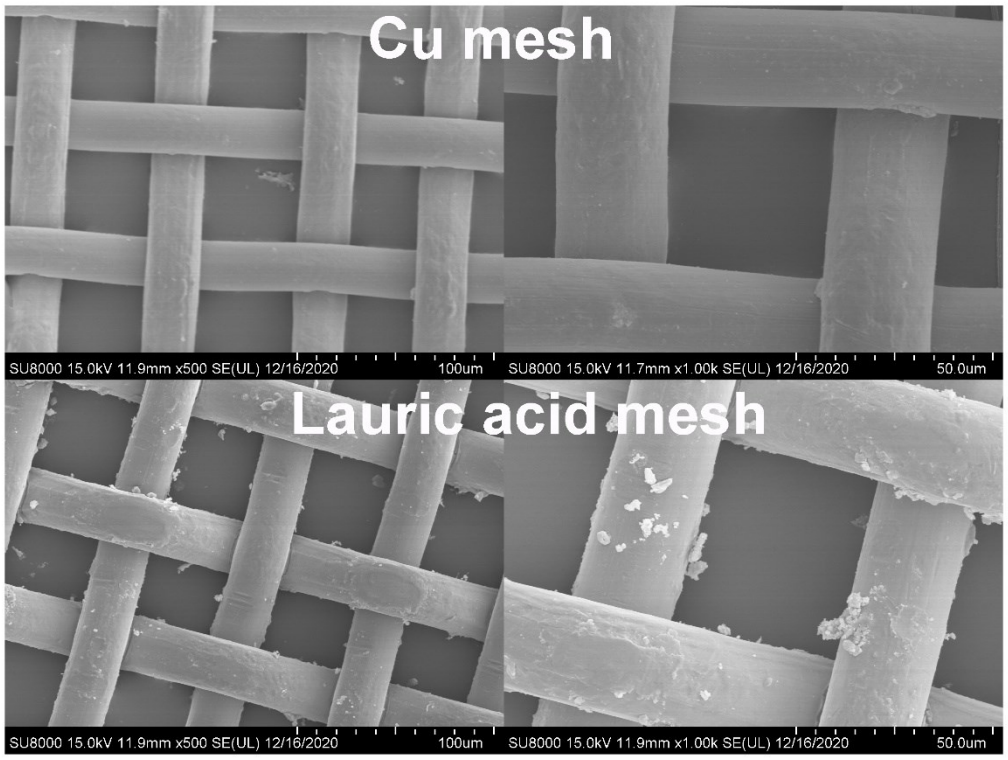

Fig. S12. FESEM images of lauric acid-mesh and Cu substrate.

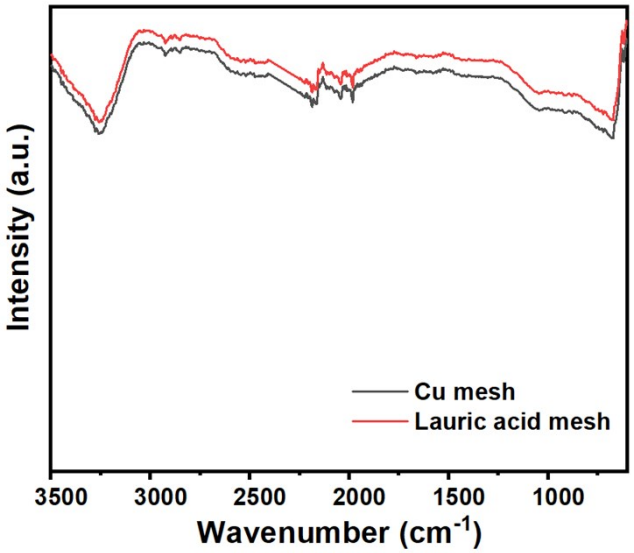

Fig. S13. FTIR spectra of lauric acid-mesh and Cu substrate.

Fig. S14. The largest height of water column that this V_xO_y-based dual-mesh system could stand.

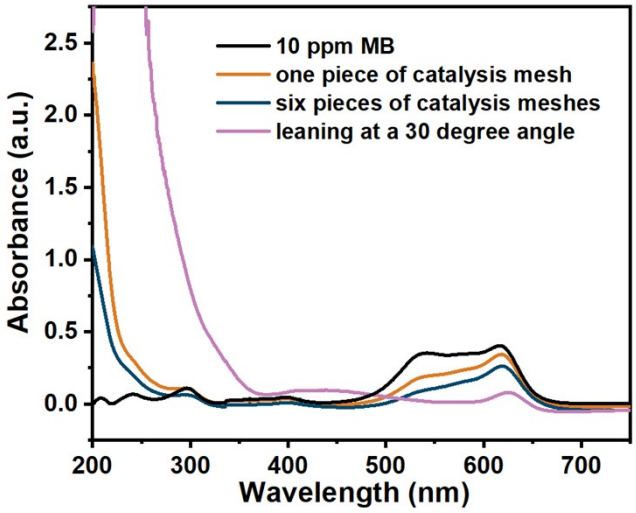

Fig. S15. UV-Vis spectra of 20 mL 10 ppm MB solution treated by three control tests, respectively.

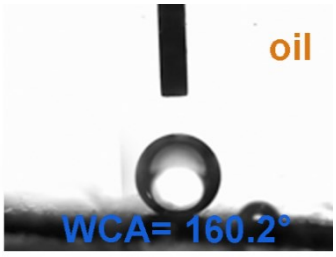

Fig. S16. WCA of catalysis mesh under oil.

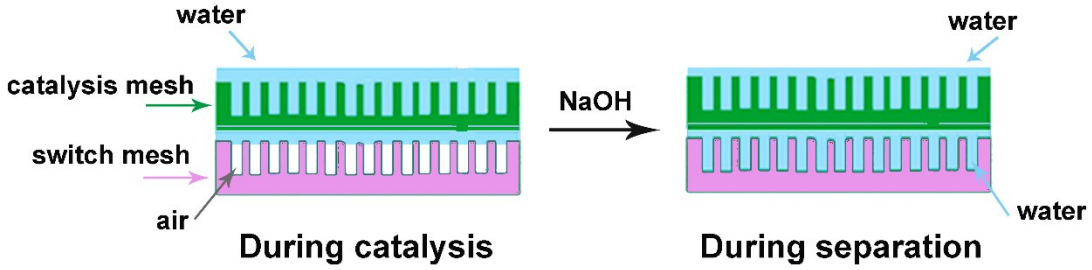

Fig. S17. The transformation of wetting states during the process of catalysis and subsequent separation, initial air gaps between the catalysis and switch meshes during catalysis were then be replaced by water during separation.

Discussion: When the catalysis and switch meshes were applied into controllable degradation and subsequent separation, in the beginning the switch was "off" for conducting complete catalysis. In this process, the catalysis was superhydrophillic, in other words, with a Wenzel totally infiltrated state and therefore with no air cushion in catalysis mesh. In contrast, the switch mesh was superhydophobic, in other words, with a Cassie state where air was trapped into the micro structures. Therefore, when the switch mesh was off, there might be some air gap between the catalysis and switch meshes. This air gap contributes to the superhydrophobicity of the switch mesh and in fact conduces to the catalysis process because this helps the system to bear a larger volume of target solutions.

When the process was moved forward to the separation procedure, the switch mesh was adjusted to "on" state through alkaline solution. In this process, the switch mesh was transformed from a superhydrophoic state to a superhydrophillic state, which was from a Cassie state to a Wenzel state indeed. Concretely, when adjusted by alkaline solution, the carboxyls coordinated with vanadium atoms were cleaved and dodecanoates were formed on the surface. Subsequently, water molecules would penetrate through the array of alkyl chains and displace the air cushion in the micro structure of the switch mesh, as a result achieving a totally superhydrophillic wetting state. In this way, the air between the catalysis and switch meshes would be replaced by water and disappear, with which state the separation could be conducted more fluently and efficiently. In conclusion, the changes of air gaps between the catalysis and switch meshes have been conductive to both the catalysis and separation procedures.

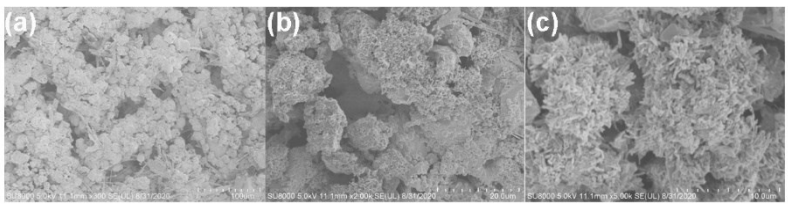

Fig. S18. SEM images of catalysis mesh after five iterations of simultaneous removal of organic pollutants and oil phase.

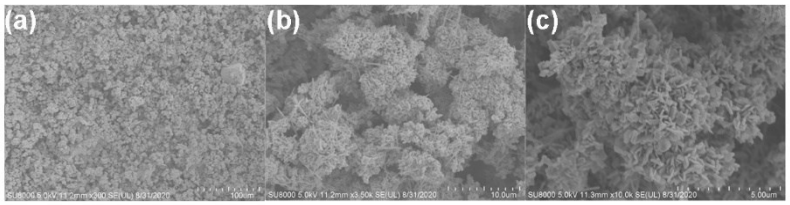

Fig. S19. SEM images of switch mesh after five iterations of simultaneous removal of organic pollutants and oil phase.

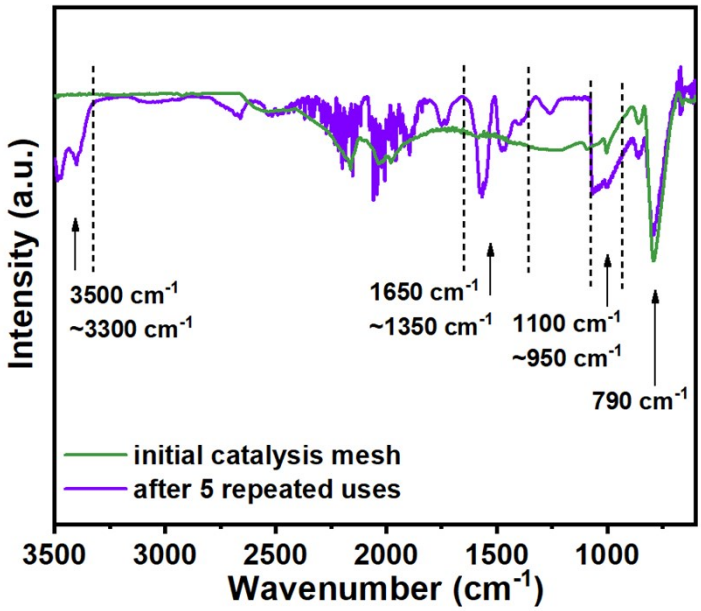

Fig. S20. FTIR spectra of the catalysis mesh after five iterations of simultaneous removal of organic pollutants and oil phase.

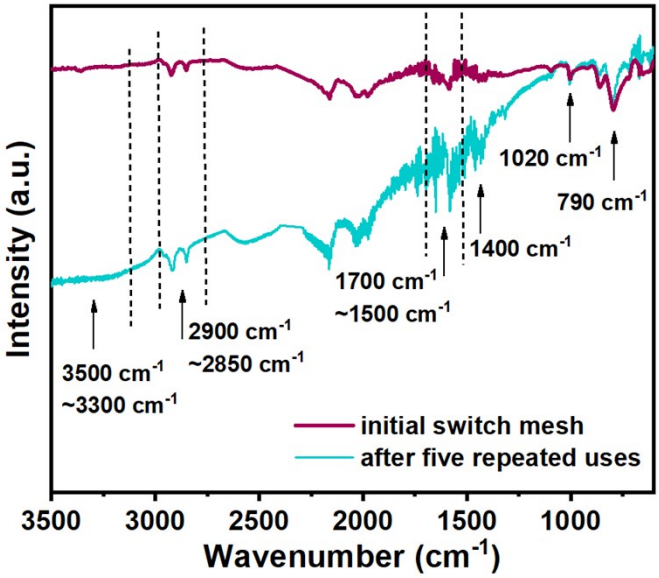

Fig. S21. FTIR spectra of the switch mesh after five iterations of simultaneous removal of organic pollutants and oil phase.

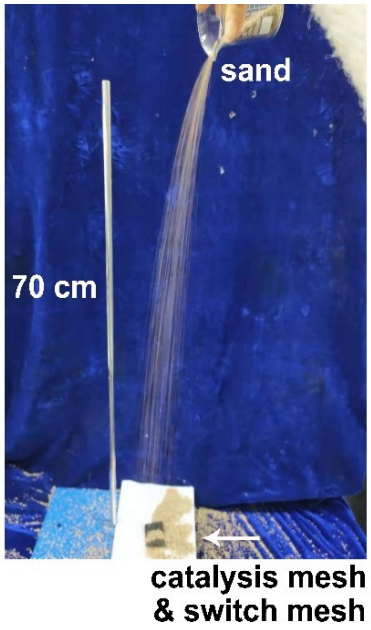

Fig. S22. Mechanical durability test of catalysis mesh/ switch mesh composite system.

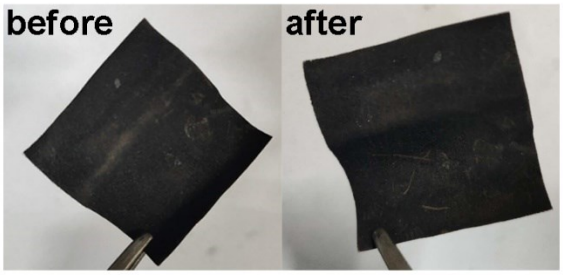

Fig. S23. Photos of the catalysis mesh before and after the mechanical durability test.

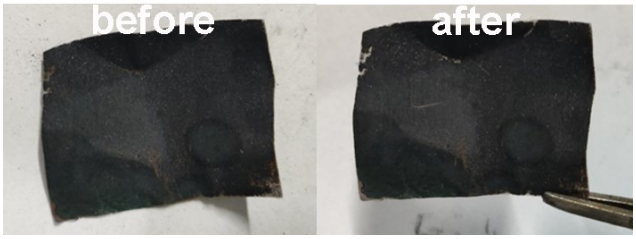

Fig. S24. Photos of the switch mesh before and after the mechanical durability test.

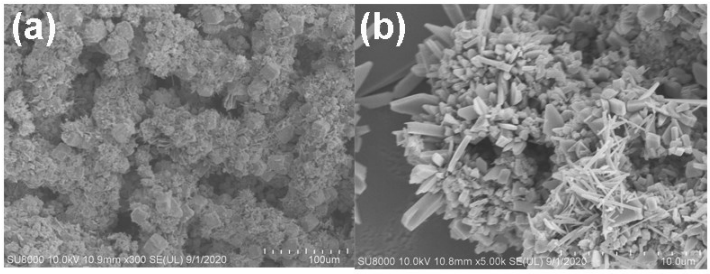

Fig. S25. SEM images of the catalysis mesh before and after the mechanical durability test.

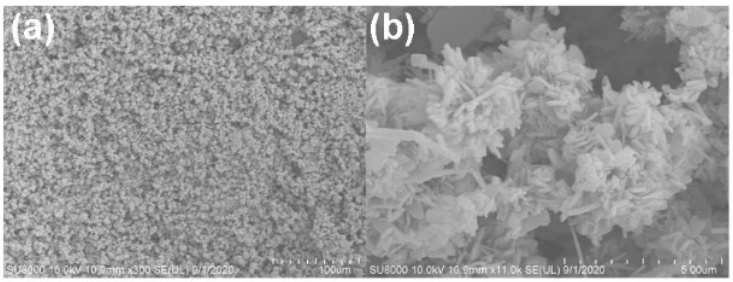

Fig. S26. SEM images of the switch mesh before and after the mechanical durability test.

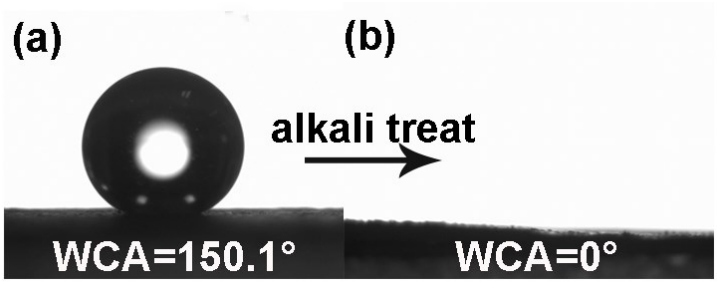

Fig. S27. Wettability transformation of the switch mesh before and after the mechanical durability test.

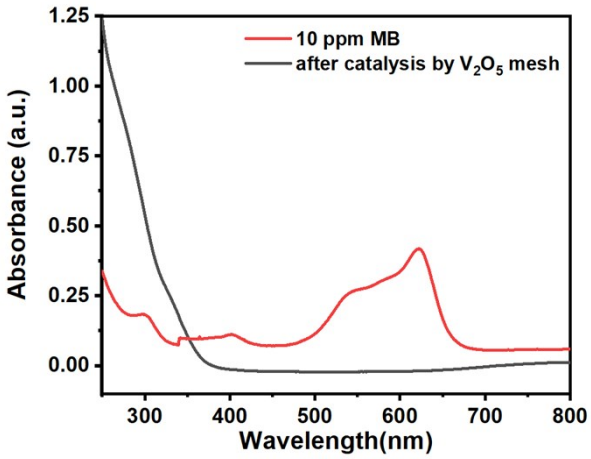

Fig. S28. UV-Vis spectra of 10 ppm MB degraded by the catalysis mesh before and after the mechanical durability test (in activation of 2.0 g/L PMS).

Movie S1. The switch mesh shows water repellency towards acid solution (pH= 2).

Movie S2. The switch mesh shows water repellency towards neutral solution.

Movie S3. The rapid response of the switch mesh towards basic solution (pH= 12).